International Journal of Nanoelectronics and Materials
Volume 16 (Special Issue) December 2023 [347-359]

Enhancement of Structural and Optical Characteristics of Nanostructured InGaN Using Electrochemical Etching

Anis Nabilah Mohd Daud[1], Rosfariza Radzali[1,*], Ainorkhilah Mahmood[2], Zainuriah Hassan[3], Alhan Farhanah Abd Rahim[1], Muhammad Fadhirul Izwan Abdul Malik[4], Mohd Hanapiah Abdullah[1], and Emilia Noorsal[1]

[1]Electrical Engineering Studies, College of Engineering, Universiti Teknologi MARA, Cawangan Pulau Pinang, 13500 Permatang Pauh, Pulau Pinang, Malaysia
[2]Department of Applied Science, Universiti Teknologi MARA, Cawangan Pulau Pinang, 13500 Permatang Pauh, Pulau Pinang, Malaysia
[3]Institute of Nano Optoelectronics Research and Technology (INOR), Universiti Sains Malaysia, 11800 USM, Penang, Malaysia
[4]Science and Engineering Research Centre (SERC), Universiti Sains Malaysia, Engineering Campus, 14300 Nibong Tebal, Penang, Malaysia

ABSTRACT

In this work, we used an alternating current electrochemical etching technique to fabricate nanostructured InGaN in potassium hydroxide, which serves as an electrolyte. The effects of different current densities during alternating current electrochemical etching on the morphological and optical characteristics of the nanostructured InGaN samples were investigated. The morphology of the nanostructured InGaN samples was determined by extreme high resolution field emission scanning electron microscopy. The pore size (~38 nm) and estimated porosity (~35%) were highest at 250 mA/cm² current density. Furthermore, the surface roughness and average pore depth of the nanostructured InGaN increased with increasing current density, as revealed by atomic force microscopy. X-ray diffraction data showed a reduction in the full width at half maximum value and dislocation density of the nanostructured InGaN samples. The InGaN-like E_2(high) phonon mode of the nanostructured InGaN sample was shifted to a higher frequency in the Raman spectra relative to that of the untreated sample, indicating that stress relaxation occurs in the nanostructured samples. Raman spectra showed an increase in intensity of the nanostructured InGaN samples showing improvement in optical property. The observed properties illustrate the potential of using nanostructured InGaN application in sensing devices.

Keywords: Nanostructured, InGaN, alternating current, electrochemical etching

1. INTRODUCTION

Nanostructured III-nitrides, such as nanostructured indium gallium nitride (InGaN), have receives a lot of interest in recent years because of their distinctive characteristics, for example, large band gap and outstanding thermal, and mechanical stability [1]. Nanostructured InGaN has large surface area-to-volume ratio that can improve the physical and optical properties required for sensing devices. Nanostructures can also act as a growth template, which can provide stress relaxation leads to a reduction in defects such as dislocation density for the subsequent growth template [2]. Another advantage of nanostructures is their ability to increase the luminescence intensity, which makes them a promising option for optoelectronic devices [3].

* Corresponding authors: rosfariza074@uitm.edu.my

Moreover, wet etching technique such as electroless etching and direct current electrochemical etching has been utilized to fabricate III-nitride nanostructured samples. Wet etching is a relatively simple and inexpensive technique that is often used to fabricate nanostructures on semiconductors. A chemical solution or electrolyte is usually used during the wet etching process. Electroless etching is catalysed by metals and does not require an external power source [4]. Instead, it requires oxidising agents that are capable of injecting holes into the semiconductor's valence band. However, this techniques tends to generate small and non-uniform pores or nanostructures [4, 5]. In contrast, direct current electrochemical etching involves etching the III-nitride sample in a potassium hydroxide (KOH) electrolyte using a constant direct current (DC) source [6, 7]. Nevertheless, the DC applied throughout the etching process creates nitrogen bubbles, which can attach to the InGaN surface and slow down the etching rate [8-10], resulting in non-uniform and low pore density and porosity of the nanostructured InGaN [11]. To address these issues, alternating current can be applied for electrochemical etching to improve the etching rate and subsequently increase the pore density and porosity of the nanostructured InGaN. The alternating current electrochemical etching technique that uses alternating current (AC) can minimize the creation of nitrogen bubbles throughout the cathodic half cycle, and it enables fresh KOH molecules to interact with the InGaN surface to create nanostructures during the anodic half cycle [10, 12].

In this study, we fabricated nanostructured InGaN samples using the alternating current electrochemical etching technique. KOH electrolyte was used to etch the InGaN sample at different current densities of the AC power supply. The study of nanostructured InGaN fabricated using alternating current during electrochemical etching is at the beginning stage of development. Therefore, not all fundamental characteristics have been explored. Therefore, the effect of varying current densities during the electrochemical etching on the characteristics of the nanostructured InGaN were characterized using extreme high resolution field emission scanning electron microscopy (XHR-FESEM), energy dispersive x-ray spectroscopy (EDX), atomic force microscopy (AFM), x-ray diffractometer (XRD), and Raman spectroscopy.

2. MATERIAL AND METHODS

2.1 Sample Preparation

A commercial unintentionally doped $In_{0.1}Ga_{0.9}N$ wafer was used to fabricate nanostructured InGaN samples. The InGaN layer was 300 nm thick, and that of the GaN layer was 3.2 µm thick. Prior to the etching process, the InGaN sample was cleaved into small pieces via a diamond scriber. The InGaN wafer structure is presented in Figure 1.

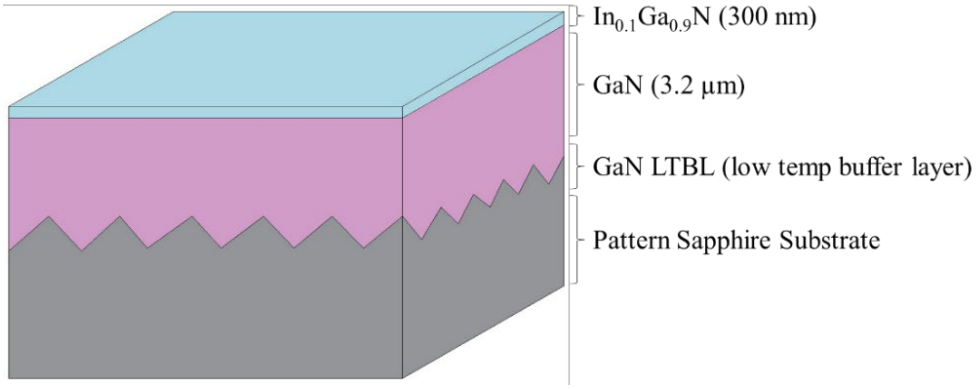

Figure 1. Schematic diagram of the as-grown InGaN structure.

2.2 Formation of Nanostructured InGaN

Figure 2 depicts the experimental setup to fabricate nanostructured InGaN samples via alternating current electrochemical etching. The sample was etched in a KOH electrolyte in a custom-made Teflon cell under illumination provided by a 400 W ultraviolet light. KOH is a common electrolyte used to fabricate nanostructures of III-nitride semiconductors [13, 14]. During the alternating current electrochemical etching process, InGaN samples were applied with AC at 100, 150, 200, or 250 mA/cm^2 current densities with a constant etching duration Following the etching procedure, the samples underwent careful cleaning with deionized (DI) water before being allowed to air-dry at room temperature.

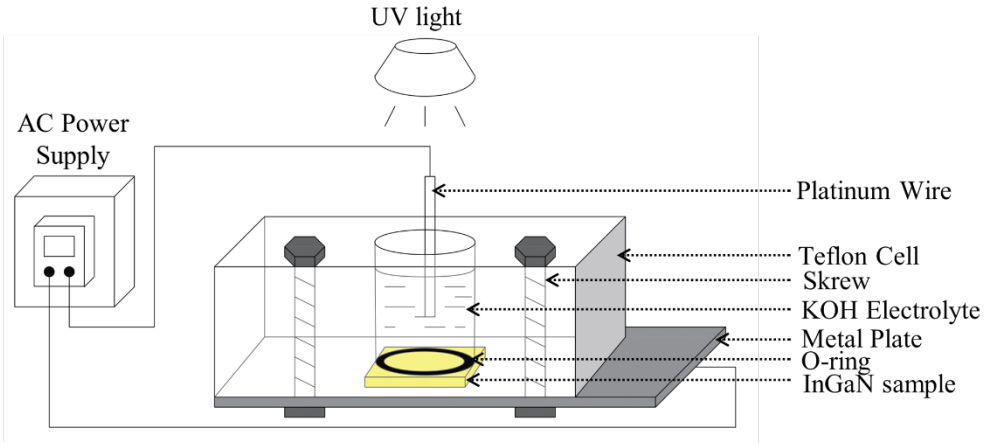

Figure 2. Schematic diagram of the alternating current electrochemical etching technique.

2.3 Characterization of the Samples

XHR-FESEM and EDX (FEI Verious 460L, United States, 2015) were used to characterize the surface morphology of the samples, while AFM (Dimension Edge, Bruker, German, 2011) were utilized to obtain the surface roughness and estimated average pore depth with the scan area of 5 × 5 μm^2. In addition, phase analysis was performed on all samples using a XRD (PANalytical PRO DY 2536, Netherlands, 2007). The optical properties of the samples were characterized using a Raman spectrometer (Renishaw inVia, The United Kingdom, 2010). The laser used for Raman measurements was 20 mW HeNe laser (λ = 633 nm).

3. RESULTS AND DISCUSSION

3.1 XHR-FESEM

The efficiency of electrochemical etching is based on the electron-hole pairs generated by photon absorption, as the etching process causes oxidation followed by dissolution on the semiconductor surfaces [15]. Upon illumination, electrons in the valence band jump to the conduction band and generate holes in the valance band [16]. In this study, when the InGaN surface was immersed in the KOH electrolyte, the energy band at the interface of InGaN/KOH electrolyte exhibited upward bend bending (Figure 3), which caused the holes to accumulate at the sample surface [17]. Throughout the negative half cycle of the AC, the electrons were forced through the interface to the electrolyte [18]. The accumulation of electrons at the platinum (Pt) electrode, which takes place in the electrolyte, led to a reduction reaction of the water molecules, which resulted in the formation of hydrogen gas [19]. On the other hand, at the positive half cycle of the AC, holes drifted towards the InGaN surface [18]. This process led to an increment in the amount of electrons going to the Pt electrode and enhanced the number of holes that accumulating on the

InGaN surface. The holes assist in changing the surface atoms to a greater oxidation state, hence, favouring oxidative decomposition [16, 20]. Therefore, chemical attack occurs at the InGaN surface that has become positively charged. The decomposition of InGaN then leads to the formation of nitrogen gas. Following that, the oxide layer that dissolves in the KOH solution leads to the generation of nanostructures. The generation of nanostructures on the InGaN surface due to the electrochemical etching can be visually confirmed by XHR-FESEM images. In addition, the application of AC for electrochemical etching can decrease the creation of nitrogen bubbles throughout the cathodic half cycle while allowing fresh KOH molecules to react with InGaN during the anodic half cycle, which can significantly increase the etching activity. In this study, we varied the AC current density to control the formation of nanostructures, pore size, and pore density in the nanostructured samples.

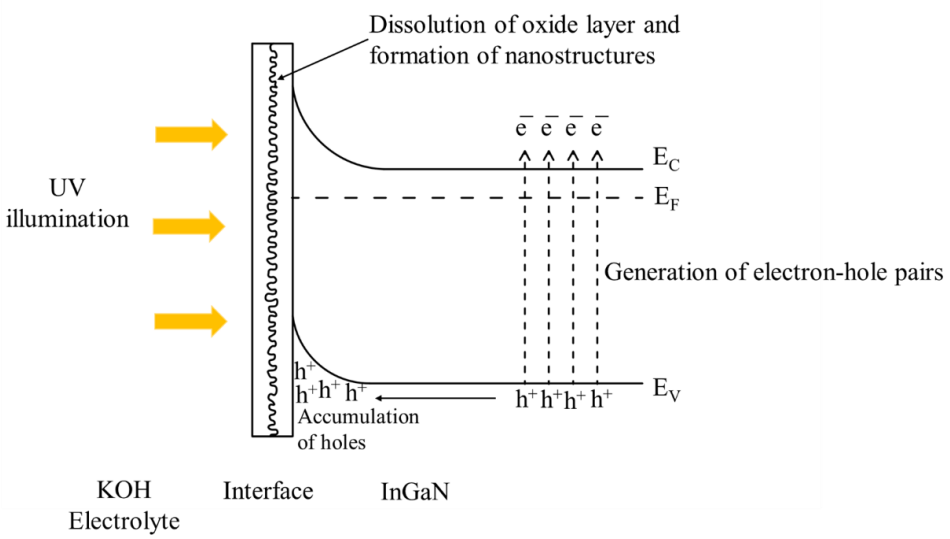

Figure 3. A schematic diagram of the formation of nanostructured InGaN and energy band diagram at InGaN surface/KOH electrolyte that shows upward bend bending.

The XHR-FESEM images of the nanostructured InGaN samples fabricated via alternating current electrochemical etching technique under various current densities are presented in Figure 4 and the relationship between the average pore size and the estimated porosity of the nanostructured InGaN samples on current density is displayed in Figure 5. By using ImageJ software, the number of pixels of the total surface area of the XHR-FESEM image and pore area were counted in order to estimate the percentage of porosity. The ratio between the total pore area and the total surface area was then calculated as the estimated porosity [21, 22].

Figure 4a depicts the surface morphology of the as-grown InGaN sample, which displays smooth surface morphology. Therefore, the average pore size and estimated porosity were not calculated for this sample. The average pore size and estimated porosity for the nanostructured sample etched at 100 mA/cm^2 were ~12 nm and ~22%, respectively (Figure 4b). The values of this structure closely resembled the value of nanostructured InGaN reported previously [11].

When the current density increased, the nanostructured InGaN underwent some morphological changes. At 150 mA/cm^2, the pore size of the nanostructured InGaN was larger than that of the 100 mA/cm^2 sample (Figure 4c). Additionally, the formation of circular pore structure was more pronounced, with average pore size increasing to ~18 nm and estimated porosity to ~24%, indicating that the size of pores increased as the current density increased. Furthermore, the 200 mA/cm^2 sample (Figure 4d), the pore size ~22 nm and the porosity ~28% further increased compared to the 100 and 150 mA/cm^2 samples.

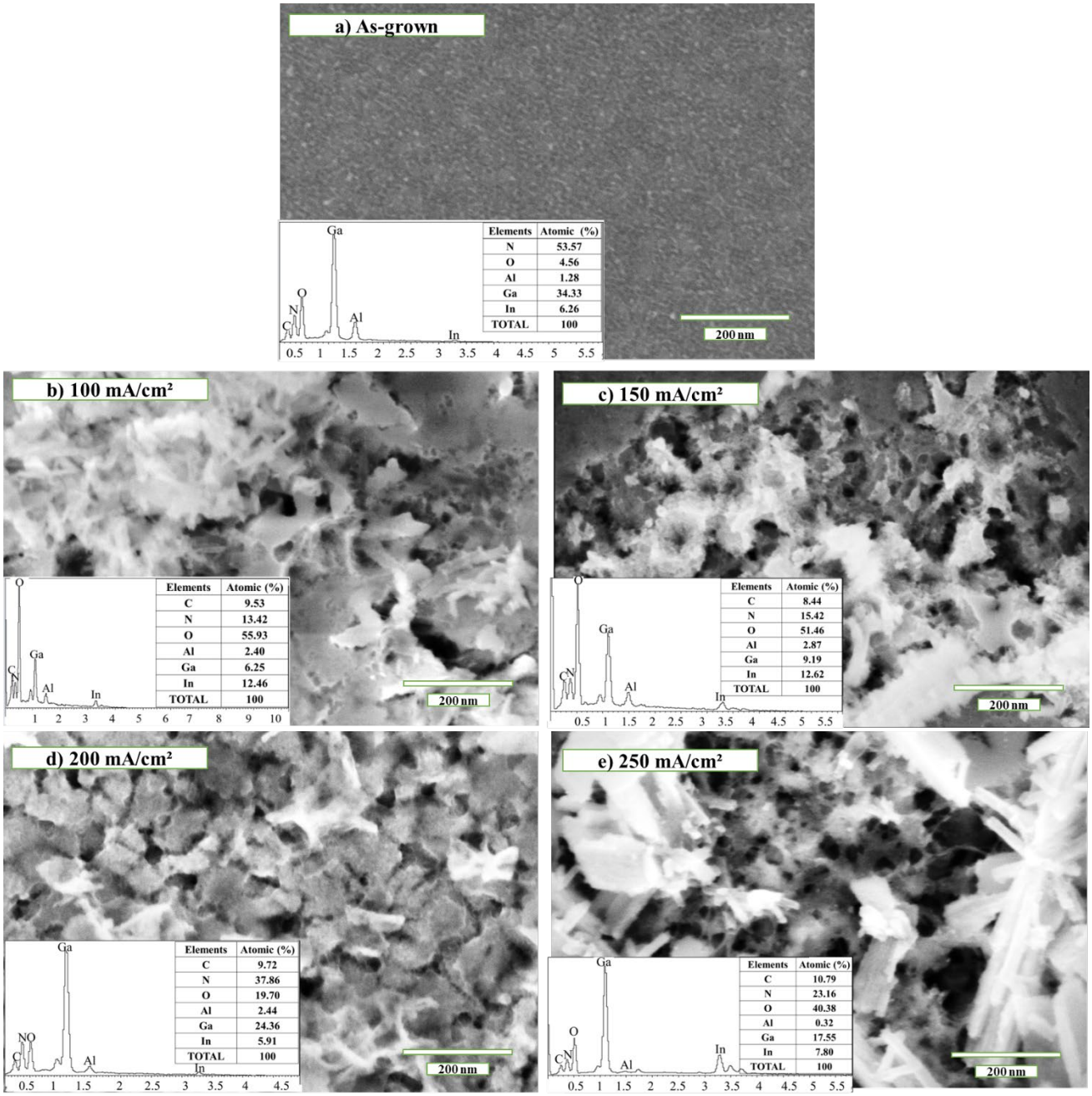

Figure 4. XHR-FESEM images of as-grown and nanostructured InGaN samples subjected to alternating current electrochemical etching at various current densities: (a) as-grown, (b) 100 mA/cm^2, (c) 150 mA/cm^2, (d) 200 mA/cm^2, and (e) 250 mA/cm^2.

When the current density was 250 mA/cm^2, the nanostructures became even more pronounced (Figure 4e), and the pore density increased along with pore size. Therefore, the pore size, density, and porosity increased with increasing current density. The average pore size of the nanostructured InGaN sample etched at current density of 250 mA/cm^2 was ~38 nm, and its estimated porosity was ~35%, which was the highest among the samples analysed in this study. The high pore density and porosity of this sample could be associated with the etching process of the alternating current electrochemical etching technique.

The AC that operated in both positive and negative cycles helped to reduce the amount of nitrogen bubbles that generated during the cathodic half cycle and allowed fresh KOH molecules to react with InGaN surface during the anodic half cycle, which can significantly increase the etching activity [8, 10, 12, 23]. Thus, this technique mitigated the problem of nitrogen bubbles lowering the etching rate and resulted in increased pore size, density, and porosity of the nanostructured InGaN samples.

Furthermore, we previously fabricated nanostructured InGaN via direct current electrochemical etching [7, 11]. However, the nanostructured InGaN exhibited lower pore density relative to the nanostructured InGaN fabricated via alternating current electrochemical etching in the current study. The low pore density of the former samples could be due to the presence of nitrogen bubbles [9, 10, 24]. This comparison illustrates that the alternating current electrochemical etching is better than the direct current electrochemical etching at producing a nanostructured InGaN with higher pore density and porosity, which are properties required for application in gas sensors and photodetectors.

We also used EDX to measure the atomic values of the elements in the thin films, as the peak intensity in the EDX spectrum provides information about the atomic composition and concentration of the elements present in the sample. The EDX measurement showed that the nanostructured InGaN samples still contained In, which indicates that the InGaN layer was still present and not entirely removed due to the etching process.

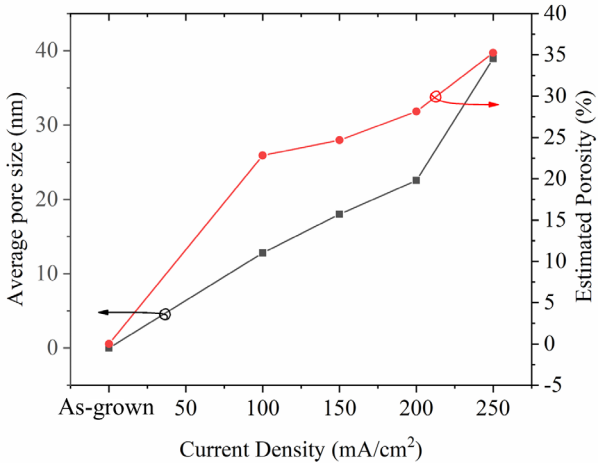

Figure 5. Relationship between average pore size and estimated porosity with respect to current density.

3.2 AFM

The AFM was utilized to measure the surface roughness in root-mean-square (RMS) of as-grown and nanostructured InGaN samples etched at various current densities via alternating current electrochemical etching (Figure 6) and Figure 7 shows the relationship between RMS surface roughness and estimated average pore depth on current density. The section line scan function in the AFM NanoScope Analysis software was employed to determine the estimated average pore depth of the nanostructured InGaN sample. Other researchers have used similar non-destructive techniques to determine the estimated average pore depth of their nanostructured samples [8, 25, 26].

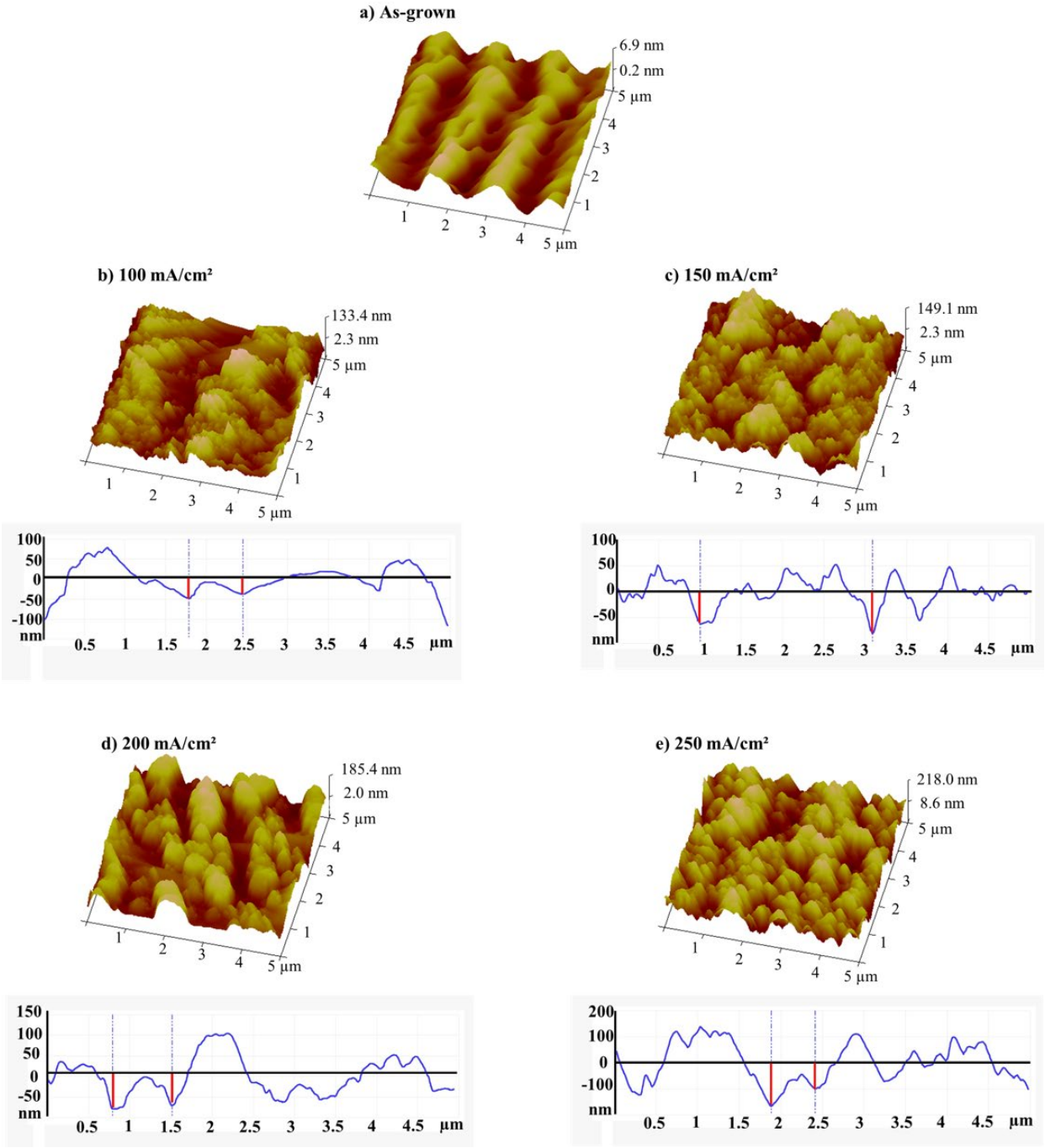

Figure 6. AFM measurements and cross-section line scan of as-grown and nanostructured InGaN samples subjected to alternating current electrochemical etching under various current densities: (a) as-grown, (b) 100 mA/cm^2, (c) 150 mA/cm^2, (d) 200 mA/cm^2, and (e) 250 mA/cm^2.

The as-grown InGaN sample had surface roughness of 2.23 nm, indicating a smooth surface. However, the etching process increased the surface roughness of the nanostructured InGaN samples. The sample obtained by etching at 100 mA/cm^2 had a surface roughness value of 36.10 nm and an estimated average pore depth of 32.01 nm, which were higher than those of the as-grown sample (Figure 6b). Furthermore, for the 150 mA/cm^2 sample (Figure 6c), the surface roughness was measured to be 42.20 nm and the estimated average pore depth was 42.18 nm.

Moreover, increasing the current density to 200 mA/cm² (Figure 6d) also resulted in increased of surface roughness (56.0 nm) and the estimated average pore depth (72.04 nm). At 250 mA/cm² (Figure 6e), the surface roughness (65.4 nm) and estimated average pore depth (75.98 nm) were highest among the nanostructured InGaN samples. The RMS values and estimated average pore depth of the nanostructured InGaN samples increased proportionally to the current densities applied during the etching process (Figure 7). These observations were confirmed by the XHR-FESEM images (Figure 4), which clearly show that the morphology of the InGaN film gradually changed when the current density increased due to the effect of the alternating current electrochemical etching process on the surface and structure of the film. Quah et al. [27] reported identical results, which confirms that increasing the current density increases the RMS surface roughness in the nanostructured sample.

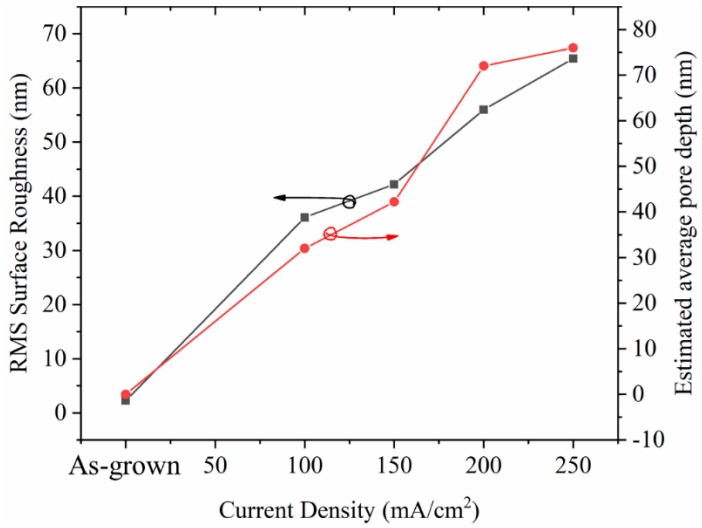

Figure 7. Relationship between RMS surface roughness and estimated average pore depth on current density.

3.3 XRD

The XRD patterns for the as-grown and nanostructured InGaN samples etched at various current densities are shown in Figure 8. For the as-grown InGaN sample, the peaks that were associated with InGaN (0002), GaN (0002), InGaN (0004), and GaN (0004) were observed at 34.14°, 34.85°, 73.04°, and 73.26°, respectively. The peak detected at 41.91° was attributed to the sapphire substrate. Furthermore, the (0002)-oriented InGaN diffraction peaks shifted to a higher diffraction angle in the nanostructured InGaN samples with respect to the as-grown sample. The diffraction peaks of InGaN (0002) were shifted to higher angle after etching for 100 mA/cm² (34.18°), 150 mA/cm² (34.16°), 200 mA/cm² (34.25°), and 250 mA/cm² (34.26°). Additionally, the (0002)-oriented InGaN diffraction peaks were shifted nearer to the (0002)-oriented GaN diffraction peak, indicating the change of In in the InGaN film and closer composition of the InGaN film to that of GaN [3, 13, 28].

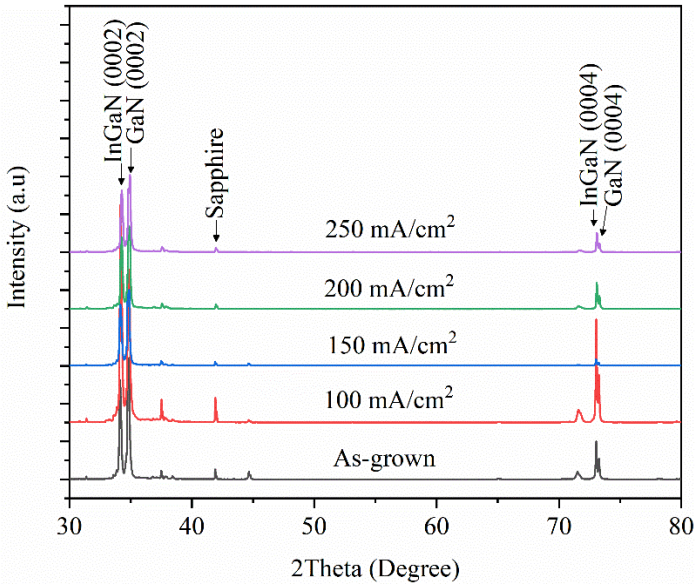

Figure 8. XRD patterns of the as-grown and nanostructured InGaN samples.

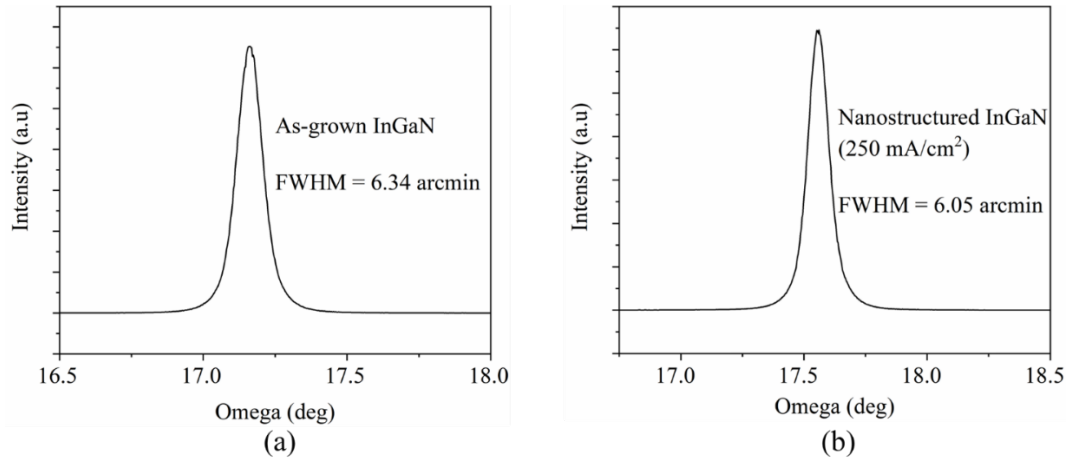

Figure 9. ω-scans of the XRD rocking curves (RC) at the (0002) plane of (a) as-grown and (b) nanostructured InGaN samples etched at 250 mA/cm².

We determine the crystalline quality of all investigated samples by conducting ω-scans of the XRD rocking curves (RC). The RC measurement was conducted at the symmetric (0002) plane. Figure 9 shows the RC for as-grown and 250 mA/cm² sample. The FWHM of the RC was used to calculate the estimation of $N_{screw+mixed}$ dislocation density and the crystalline quality of all the samples can be investigated [29]. Hence, the $N_{screw+mixed}$ can be calculated by taking into consideration FWHM of the RC and c-type Burger's vector via the following equation [30]:

$$N_{screw+mixed} = \frac{\beta^2_{(0002)}}{4.35 \times b_c^2}$$

where $\beta_{(0002)}$ is the FWHM of the (0002) scan and b_c is the Burger vector of the c-type threading dislocation. Using Vergard's law, the Burger vectors of $In_{0.1}Ga_{0.9}N$ were estimated from the Burger vectors of GaN (b_c = 0.5185 nm) and InN (b_c = 0.5703 nm) [31].

Moreover, Figure 10 shows the dependence $N_{screw+mixed}$ dislocation density of as-grown and nanostructured InGaN on current density. It is interesting to note that nanostructured InGaN samples had lower FWHM value for RC at the symmetric (0002) plane with respect to the as-grown InGaN sample reflecting lower $N_{screw+mixed}$ dislocation density which is better crystalline quality of the nanostructured InGaN samples–[15]. We observed that the FWHM value and estimated $N_{screw+mixed}$ dislocation density decreased in nanostructured InGaN samples with the increasing of the etching current density. Furthermore, among the nanostructured InGaN samples, the FWHM of the RC (0002) and the estimated $N_{screw+mixed}$ dislocation density of the 250 mA/cm^2 etched sample exhibited the lowest values as shown in Figure 10. This result indicated that the alternating current electrochemical etching helped to remove the dislocation defects and improved the crystalline quality of the nanostructured InGaN samples [7, 29]. However, the FWHM value for the 150 mA/cm^2 sample was slightly higher than that of the untreated sample, but the increase was only 0.16 arcmin (9.6 arcsec). This suggests that the quality of the 150 mA/cm^2 etched sample was as good as that of the as-grown sample. Vajpeyi et al. [15] reported a similar amount of increase in FWHM for their nanostructured sample. The increase in FWHM and dislocation density of the 150 mA/cm^2 sample relative to the as-grown sample may be due to the incorporation of impurity-induced disorders or surface damage and formation of non-stoichiometric surfaces during the etching process [7, 15].

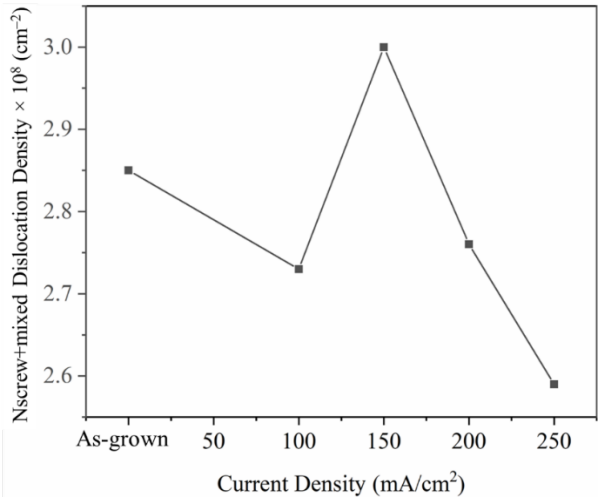

Figure 10. Dependence of Nscrew+mixed dislocation density of as-grown and nanostructured InGaN on current density.

3.4 Raman Spectroscopy

Figure 11 presents the Raman spectra of as-grown and nanostructured InGaN samples. Optical phonons belonging to GaN E_2(high) at 569 cm^{-1} and GaN A_1(LO) were identified at 734 cm^{-1} for all of the investigated films. The presence of an additional peak at 561 cm^{-1} (inset Figure 11) between the E_2(high) phonon mode of GaN and the E_2(high) phonon mode of InN was attributed to the InGaN-like E_2(high) phonon mode. The assignment of the InGaN-like E_2(high) phonon mode was referred to previous reports in [16, 32, 33].

The phenomenon of more light interaction in the nanostructured InGaN sample due to the surface disorder had resulted in a significant increase in Raman intensity in all of the nanostructured InGaN samples compared to the untreated sample [34]. Similar observation has been reported in [6]. The enhancement of optical properties provides important insights for the potential use of nanostructured InGaN in optoelectronic applications such as photodetectors.

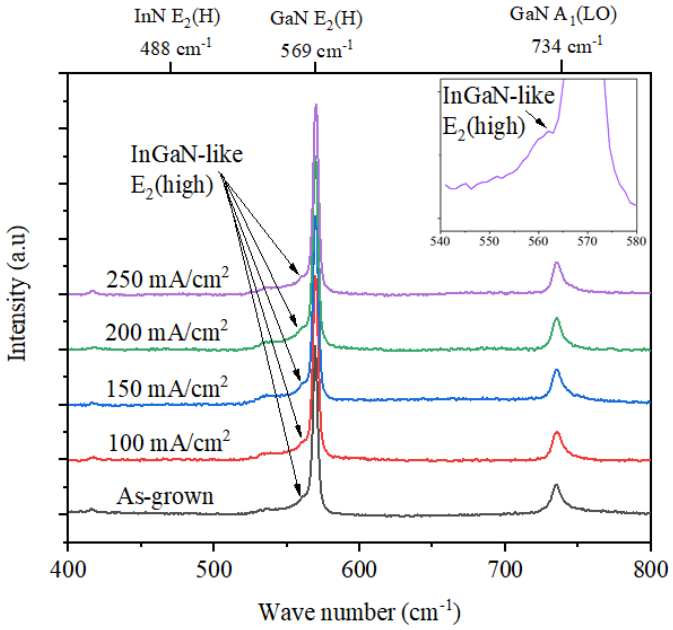

Figure 11. Raman spectra of as-grown and nanostructured InGaN samples. The inset figure depicts the zoom-in of the Raman spectra at around 561 cm^{-1}.

Overall, we detected a peak shift of the InGaN-like E_2(high) phonon mode to a larger wave number for all nanostructured samples in relative to the as-grown sample. This result suggests that stress relaxation occurred in the nanostructured samples obtained by electrochemical etching. Therefore, the amount of stress relaxation can be calculated by analysing the shift of the InGaN-like E_2(high) phonon mode of the nanostructured sample with respect to the as-grown sample as follows: $\Delta\omega_{E_2} = K_R\sigma$ where K_R and σ refer to the proportionality factor and the in-plane biaxial stress, respectively. Meanwhile the proportionality factor of InGaN was estimated by linear interpolation from the proportionality factor of GaN = 4.2 cm^{-1} GPa^{-1} [35] and InN = 9.0 cm^{-1} GPa^{-1} [36].

Moreover, Figure 12 depicts the dependence of amount of stress relaxation on current density. We observed that the amount of stress relaxation decreased with the increase in applied current density. The decreasing trend of the amount of stress relaxation was consistent with the increasing trend in pore size and pore density shown in the XHR-FESEM results. Vajpeyi et al. [34] noted that the amount of stress relaxation was affected by the pore size of the nanostructure, as they observed larger pore size in the nanostructure with a lower amount of stress relaxation.

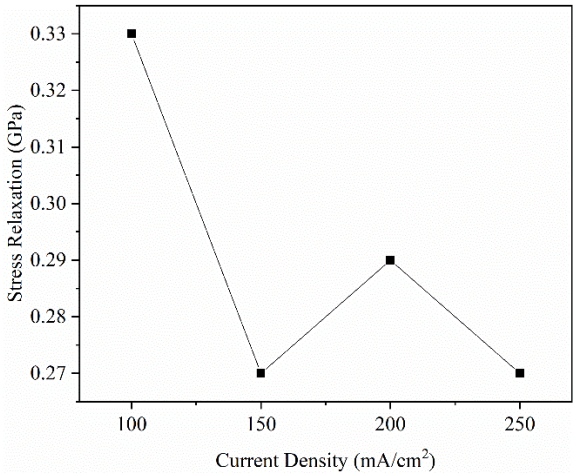

Figure 12. Dependence of amount of stress relaxation of nanostructured InGaN on current density.

4. CONCLUSION

Alternating current electrochemical etching of InGaN films was performed in a KOH electrolyte solution at various current densities (100, 150, 200, and 250 mA/cm^2). The results showed that current density affected the nanostructure morphology and the structural and optical properties of nanostructured InGaN. The density of the nanostructure, porosity and pore size, as well as the surface roughness and estimated pore depth increased with current density. The FWHM and dislocation density were reduced in the nanostructured InGaN samples relative to the as-grown sample, showing that the alternating current electrochemical etching improved the quality of the nanostructured InGaN samples. Stress relaxation occurred in the nanostructured samples, and the Raman intensity of the nanostructured InGaN showed intensity enhancement, which is direct evidence of improved optical quality. Among the investigated samples, the sample etched at 250 mA/cm^2 had the highest average pore size, estimated porosity, RMS surface roughness, and estimated average pore depth as well as the lowest $N_{screw+mixed}$ dislocation density, suggesting it could be used in sensing devices.

ACKNOWLEDGEMENTS

This project was funded by the Ministry of Higher Education (MOHE) through the Fundamental Research Grant Scheme 2021 (Grant No. FRGS/1/2021/STG07/UITM/02/8). The authors also would like to thank Universiti Teknologi MARA, Cawangan Pulau Pinang, Nano-optoelectronics Research and Technology (NOR) laboratory, Institute Nano-optoelectronics Research and Technology (INOR) and Science and Engineering Research Centre (SERC) staff of Universiti Sains Malaysia for supporting this research.

REFERENCES

[1] A. Ramizy, S. H. Abud, A. S. Hussein, Z. Hassan, F. K. Yam, and C. W. Chin, Mater Sci Semicond, vol **29** (2015) pp. 102-105.
[2] J. Cui, J. Zhou, and H. Xiao, J. Alloys and Compd, vol **924** (2022) pp. 166567.
[3] R. Radzali, Z. Hassan, N. Zainal, and F. K. Yam, Sens. Actuators B: Chem, vol **213** (2015) pp. 276-284.
[4] A. P. Vajpeyi, S. Tripathy, S. J. Chua, and E. A. Fitzgerald, Phys. E: Low-Dimens., vol **28** (2005) pp. 141-149.

[5] F. Yam and Z. Hassan, Mater Lett., vol **63** (2009) pp. 724-727.
[6] H. Son, P. Uthirakumar, A. Y. Polyakov, J. H. Park, K. H. Lee, and I.-H. Lee, Appl. Surf. Sci., vol **592** (2022) pp. 153248.
[7] R. Radzali, Z. Hassan, N. Zainal, and F. K. Yam, Microelectron Eng, vol **126** (2014) pp. 107-112.
[8] F. Zulkifli, R. Radzali, A. F. Abd Rahim, A. Mahmood, N. S. Mohd Razali, and A. Abu Bakar, Microelectron. Int., vol **39** (2022) pp. 101-109.
[9] N. Naderi and M. R. Hashim, Appl. Surf. Sci., vol **258** (2012) pp. 6436-6440.
[10] A. Mahmood, Z. Hassan, A. Abd Rahim, R. Radzali, M. Ooi, and A. P. D. N. Ahmed, J. Phys. Conf. Ser., vol **1535** (2020) pp. 012006.
[11] R. Radzali, N. Zainal, F. K. Yam, and Z. Hassan, Mater Sci Semicond., vol **16** (2013) pp. 2051-2057.
[12] A. Mahmood, Int. J. Electrochem. Sci., vol **8** (2013) pp. 5801-5809.
[13] H. J. Quah, Z. Hassan, and W. F. Lim, Materials Science and Engineering: B, vol **263** (2021) pp. 114911.
[14] P. Yew, S. C. Lee, S. F. Cheah, S. S. Ng, and H. Abu Hassan, Optical Materials, vol **96** (2019) pp. 109320.
[15] A. P. Vajpeyi, ESL, vol **8** (2005) pp. G85-G88.
[16] R. Radzali, Z. Hassan, N. Zainal, and F. K. Yam, J. Alloys Compd., vol **622** (2015) pp. 565-571.
[17] M. Kaneko, H. Ueno, and J. Nemoto, Beilstein J. Nanotechnol., vol **2** (2011) pp. 127-134.
[18] H. J. Quah, N. M. Ahmed, Z. Hassan, and W. F. Lim, J. Electrochem. Soc., vol 163 (2016) p. H642.
[19] W. F. Lim, H. J. Quah, Z. Hassan, R. Radzali, N. Zainal, and F. K. Yam, J. Alloys Compd., vol **649** (2015) pp. 337-347.
[20] C. Youtsey, G. Bulman, and I. Adesida, J. Electron. Mater., vol **27** (1998) pp. 282-287.
[21] N. Astuti, N. Wibowo, and M. Ayub, Jurnal Pendidikan Fisika Indonesia, vol **14** (2018) pp. 46-51.
[22] G. D. Sulka, "Highly Ordered Anodic Porous Alumina Formation by Self-Organized Anodizing," in Nanostructured Materials in Electrochemistry, (2008), pp. 1-116.
[23] R. Radzali, M. M. Azhar, A. Mahmood, F. Zulkifli, A. Rahim, and A. A. Bakar, ASM Sci., vol **14** (2021) pp. 135-142.
[24] N. Naderi and M. Hashim, Int. J. Electrochem. Sci, vol **7** (2012) pp. 11512-11518.
[25] S. Sohimee, Z. Hassan, N. M. Ahmed, R. Radzali, H. Quah, and W. Lim, J. Phys. Conf. Ser., vol **1535** (2020) pp. 012044.
[26] P. Y. Hou, C. Van Lienden, Y. Niu, and F. Gesmundo, Quantitative assessment of pore development at Al_2O_3/FeAl interfaces during high temperature oxidation, in High Temperature Corrosion and Materials Chemistry III: Proceedings of the International Symposium, vol 2001 (2001) pp. 15.
[27] H. J. Quah, W. F. Lim, Z. Hassan, R. Radzali, N. Zainal, and F. K. Yam, Arab J. Chem., vol **12** (2019) pp. 3417-3430.
[28] S. H. Abud, Z. Hassan, and F. K. Yam, Mater. Lett., vol. **107** (2013) pp. 367-369.
[29] A. Vajpeyi, Electrochem. solid-state lett., vol **9** (2006) pp. G150-G154.
[30] S. Qu, J. Alloys Compd., vol **502** (2010) pp. 417-422.
[31] B. Gil, Group III nitride semiconductor compounds: physics and applications, (1998).
[32] M. A. Abid, H. Abu Hassan, Z. Hassan, S. S. Ng, S. K. Mohd. Bakhori, and N. H. Abd. Raof, Phys. B: Condens. Matter, vol **406** (2011) pp. 1379-1384.
[33] S. Hernández, J. Appl. Phys., vol **98** (2005) pp. 013511.
[34] A. Vajpeyi, S. Chua, S. Tripathy, and E. Fitzgerald, Appl. Phys. Lett., vol **91** (2007) pp. 083110.
[35] C. Kisielowski, Phys. Rev. B, vol **54** (1996) pp. 17745-17753.
[36] X. Wang, S.-B. Che, Y. Ishitani, and A. Yoshikawa, J. Appl. Phys., vol **99** (2006) pp. 073512.